Spring 2015

Nylon-6 Fabric Nanocomposite Resistance Temperature Detectors - Effects of Oxidant, MWCNT, and Nylon-6 Concentration

Rebecca Howdyshell
The University Of Akron, rlh63@zips.uakron.edu

Nylon-6 Fabric Nanocomposite Resistance Temperature Detectors – Effect of Oxidant, MWCNT, and Nylon-6 Concentration

Rebecca Howdyshell
The Department of Chemical and Biomolecular Engineering

Honors Research Project
April 17, 2015

Submitted to

The Honors College

Approved:	Accepted:
_____ Date 4/17/15	_____ Date 4 MAY 2015
Honors Project Sponsor (signed)	Department Head (signed)
Chelsen Montz	H. MICHAEL CHEUNG
Honors Project Sponsor (printed)	Department Head (printed)
_____ Date 4/27/15	_____ Date 4 MAY 2015
Reader (signed)	Honors Faculty Advisor (signed)
Edward A. Evans	H. MICHAEL CHEUNG
Reader (printed)	Honors Faculty Advisor (printed)
_____ Date 4/16/2015	_____ Date _____
Reader (signed)	Dean, Honors College
Gang Cheng	
Reader (printed)	

ABSTRACT

The purpose of this honors project is to construct and test temperature detectors, which can be used for the advancement of exercise devices, prosthetic sockets, or medical applications. Resistance Temperature Detectors (RTDs) are an effective way to measure temperature due to the dependence of the RTD material's resistance on temperature. The focus of this project was to develop an RTD for prosthetic socket or exercise applications, where the RTD is in close contact with the skin of the user. Generally, RTDs are constructed from platinum, copper, or nickel. However, metal RTDs have a tendency to be large and rigid, making them uncomfortable for the user. The idea for this project stems from the need for a temperature device that does not create a pressure point within the liner or shoe. Rigid temperature detectors cause pressure points, which causes wear and sores on the user, but the development of a fabric-like sensor would minimize such problems due to the thin, soft, flexible characteristics of the fabric-like RTD. A solution may have been found by adhering carbon nanotubes (CNTs) to a polymer scaffold. This project will explore the effect of varying the polymer scaffold (nylon-6 concentration in electrospinning solution), which varies the fiber diameter of the polymer, the amount of MWCNTs, and the amount and type of oxidant used before polymerization in order to create a more effective RTD of this type. This project is half of the design of experiments involving nylon-6 only. The second part of the DOE will adjust the same parameters, but use polyurethane as the scaffold rather than nylon-6 and will be completed at a later time.

A model was fitted to the data to predict temperature based on resistance. This model was compared to measured data from sensor 24A-A. Sensor 24A-A was chosen because it produced the best responses to temperature change; it displayed a linear IV curve and minimal drift and responded quickly to temperature change with minimal noise and also stabilized quickly. The average temperature difference between the model and the actual data of the entire data set was 5.66%, approximately a 1.93°C difference. The results from the parameter dependence graphs showed a possible negative correlation between percent hysteresis and MWCNT loading as well as showing a negative relation between α-value and polymer weight percent. The resistance change of both up and down ramps also appears to have a weal negative relation to polymer weight percent. The percent hysteresis graph also shows a possible positive correlation to $FeCl_3$ oxidant concentration. More analysis needs to be conducted on these aspects in order to conclude whether a correlation actually exists between these parameters.

Sensors whose resistance did not respond to temperature will be further analyzed using SEM and conductive AFM. These sensors, though non-responsive to temperature, may still respond to humidity changes, which can also be further investigated. Also, further investigation is required to determine if surfactant deposits on the MWCNTs and if so, what amount of surfactant deposits and what the effects are of this deposition.

I. Introduction

The purpose of this honors design project is to construct and test resistance temperature-detectors (RTDs) that can be used for the advancement of exercise devices, prosthetic sockets, or other medical applications. The idea for this project stems from the need of a temperature device that does not create a pressure point when used in prosthetic liners or shoes or other confined spaces close to the skin. Rigid temperature detectors, which are commonly utilized, create pressure points that causes wear and sores on the user. The development of a fabric-like sensor would minimize such problems and promote comfort, even through prolonged activity and high exertion. This paper explores the possibility of using multi-walled carbon nanotube (MWCNTs) functionalized nylon-6, with the aid of polypyrrole (PPy), as a flexible RTD.

This project is half of the design of experiments involving only nylon-6 as the scaffold. The second part of the DOE will adjust the same parameters (wt% polymer, MWCNT loading, oxidant type and concentration), but use polyurethane as the scaffold rather than nylon-6 and will be completed at a later time.

II. Background

RTD's utilize the relationship between a material's electrical resistance and temperature in order to determine temperature. The surrounding temperature can be found by measuring the electrical resistance of a material (usually by measuring the voltage drop) and applying the resistance/temperature relationship of the material [1]. Humphry Davy is credited with first discovering a relation between resistance and temperature for metals in 1821. Later, Carl Wilhelm Siemens put Davy's discovery to use by creating the first RTDs in the 1850s-60s for applications where a conventional mercury thermometer was impractical. However, RTDs were not widely used until further developed by H. L. Callendar, who researched the use of platinum and applied for his first RTD patent in 1887 [2].

Generally, RTDs are constructed from platinum, copper, or nickel. Platinum is the preferred material because of its high coefficient of resistivity and ability to maintain stability over long periods of time and is subsequently used in the International Practical Temperature Scale (IPTS). The resistance of an RTD changes with temperature following the following relationship:

Equation 1

$$R_T = R_0(1 + a_1T + a_2T^2 + a_3T^3 + \cdots + a_nT^n)$$

where,

R_T = Resistance at T °C
R_0 = Resistance at 0 °C

a_1, a_2, a_3 = constants unique to RTD material
T = Temperature °C

For industrial applications, only employing the first constant, a_1, is sufficient; the resulting relation becomes linear over a small temperature range [3]:

Equation 2

$$R_T = R_0(1 + a_1 T)$$

Recently, there has been a demand for flexible temperature sensors for medical purposes. Metal RTDs have a tendency to be larger and rigid, making them uncomfortable for the user in prosthetic sockets or when in close contact with the skin. CNTs have been found to be a promising solution when adhered to a polymer scaffold [4] [11]. Nylon-6 is a favorable polymer for the scaffold because it is already commonly used for clothing due to its tough, abrasion-resistant properties and its ability to be reinforced with other materials, such as carbon fibers [5].

Carbon nanotubes are used in temperature sensors for a number of reasons. They can be utilized on a very small scale and have high strength and sensitivity. They also consume low amounts of power and provide rapid responses. They are characterized by their high aspect ratio and electrical conductivity [6][7]. The oxidizing agents also provide sites on which the functionalization of a polymer can occur. Oxidants are used to polymerize the pyrrole to polypyrrole. $FeCl_3$ is a common oxidant used for the polymerization of pyrrole. However, there are some concerns regarding the use of $FeCl_3$ as an oxidant. The worry is that iron residue could cause polymer degradation, which could cause drift in the resistance of the sensor. Ammonium Persulfate (APS) is hoped to be used as a viable substitute as an oxidizer instead of $FeCl_3$. Polypyrrole (PPy) is a common polymer addition to CNT based sensors. Polypyrrole is used as a "connector" between nanotubes. PPy is popular due to its stability and can be synthesized easily. In addition to these characteristics, PPy is also low cost, environmentally friendly, and can have high conductivity [8][9].

III. Experimental Methods

A. DOE

The research discussed in this report consisted of half of the total DOE for the entire project. Table 1 is the total DOE for the project. It is a Taguchi L36 DOE consisting of five factors. The runs conducted for this report are listed as 1-17 in the table below, those involving nylon-6 (PA6) only. Testing regarding Polyurethane (PU) will commence during the summer of 2015.

Table 1. Total DOE for resistance temperature detectors project.

Run/Construction Order	Polymer Type	Oxidant Type	Polymer Wt%	MWCNT Amount (mg)	Oxidant Concentration (mM)
1	PA6	APS	14	1.8	25
2	PA6	APS	17	1.9	50
3	PA6	APS	20	2	100
4	PA6	APS	14	1.8	25
5	PA6	APS	17	1.9	50
6	PA6	APS	20	2	100
7	PA6	APS	14	1.8	50
8	PA6	APS	17	1.9	100
9	PA6	APS	20	2	25
10	PA6	FeCl3	14	1.8	100
11	PA6	FeCl3	17	1.9	25
12	PA6	FeCl3	20	2	50
13	PA6	FeCl3	14	1.9	100
14	PA6	FeCl3	17	2	25
15	PA6	FeCl3	20	1.8	50
16	PA6	FeCl3	14	1.9	100
17	PA6	FeCl3	17	2	25
18	PA6	FeCl3	20	1.8	50
19	PU	APS	8	1.9	25
20	PU	APS	10	2	50
21	PU	APS	12	1.8	100
22	PU	APS	8	1.9	50
23	PU	APS	10	2	100
24	PU	APS	12	1.8	25
25	PU	APS	8	2	50
26	PU	APS	10	1.8	100
27	PU	APS	12	1.9	25
28	PU	FeCl3	8	2	50
29	PU	FeCl3	10	1.8	100
30	PU	FeCl3	12	1.9	25
31	PU	FeCl3	8	2	100
32	PU	FeCl3	10	1.8	25
33	PU	FeCl3	12	1.9	50
34	PU	FeCl3	8	2	25
35	PU	FeCl3	10	1.8	50
36	PU	FeCl3	12	1.9	100

B. Chemicals and Materials

For this experiment, the materials were used as received from the supplier without further purification. Nylon-6 was obtained from Scientific Polymer Products Inc. in the form of pellets with a viscosity-average molecular weight of 10,000-grams per mole. Formic acid was received from Sigma Aldrich at a 98% purity and acetic acid from Sigma Aldrich at ≥99% purity. The multi-walled carbon nanotubes (MWCNTs) were acquired from Nanostructured & Amorphous Materials Inc. with a 10-20-nanometer diameter, 0.5-2 micrometer length, and 95% purity. The surfactant, Triton X-114, was obtained from Acros Organics. The ammonium persulfate (APS) was acquired from Sigma Aldrich and iron (III) chloride hexahydrate ($FeCl_3$•6 H_2O) with a purity of ≥98% from Flinn Scientific. Finally, the pyrrole was received from Acros Organics at ≥99% purity.

C. Electrospinning

Three different nylon-6 solutions were prepared in a 1:1 weight ratio of formic acid and acetic acid at 14-wt%, 17-wt%, and 20-wt% nylon-6. The solution was allowed to mix overnight to ensure all the nylon-6 beads had properly dissolved. The setup for electrospinning can be seen in Figure 1. The solution was drawn into the syringe barrel and connected via 1/16"ID x 1/8"OD PTFE plastic tubing (Cole Parmer Instrument Company) to a flat-tipped stainless steel syringe tip. The syringe barrel was placed onto a syringe pump set to dispense the polymer at 9.1-microliters per minute (Figure 1, label 1). The syringe tip was placed 9-centimeters from the rotating drum in a lateral spray adjustment structure by which the tip could be shifted left and right (double arrow above label 2) for uniform coverage of the collector (Figure 1, label 3). The syringe tip was adjusted approximately 2-centimeters every 2-hours. The syringe tip was connected to the positive terminal of a voltage source (Figure 1, label 2). This solution was electrospun onto a paper towel covering a copper sheet on a rotating drum. The rotating drum rotated at approximately 7-revolutions per minute, connected to a variac set to 30-volts (Figure 1, label 4). The metal structure of the rotating drum was also connected to the negative terminal of the voltage source. The material was spun for a total of 4-hours.

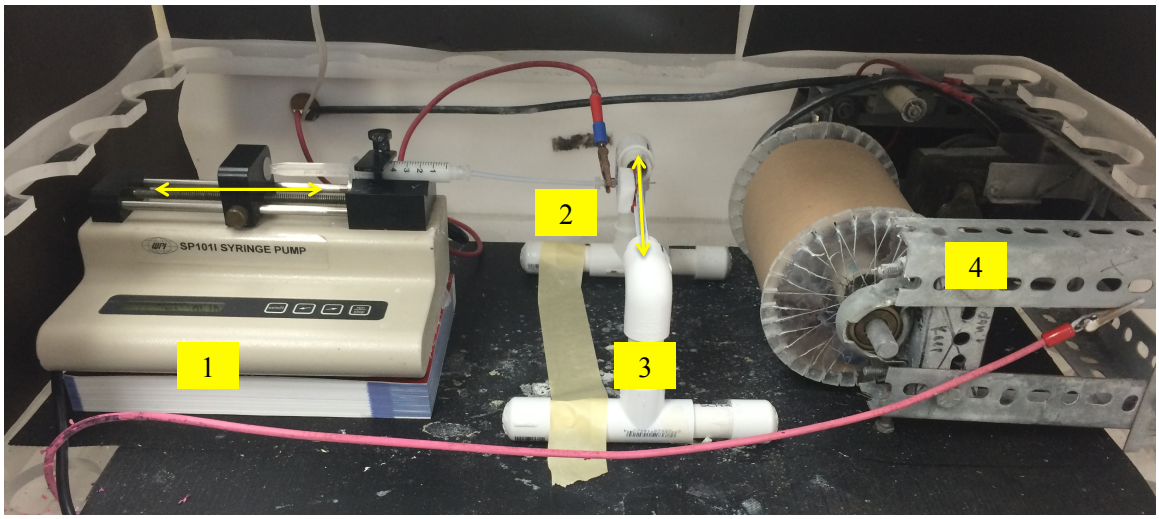

Figure 1. Electrospinning assembly. 1. World Precision Instruments Inc. (U.S.A.) SP101I syringe pump. 2. Flat-tip syringe dispensing nylon-6 connected to Gamma High Voltage Research (U.S.A.) ES30P-5W voltage source. 3. Lateral spray adjustment structure. 4. Rotating drum assembly with paper towel covered copper sheet also connected to voltage source.

D. Functionalization with MWCNTs

After spun onto the paper towel, the nylon-6 sheet was cut into discs with a 47-millimeter diameter. These discs would be functionalized with varying weights of MWCNTs. Figure 2 is a pictorial description of the functionalization process.

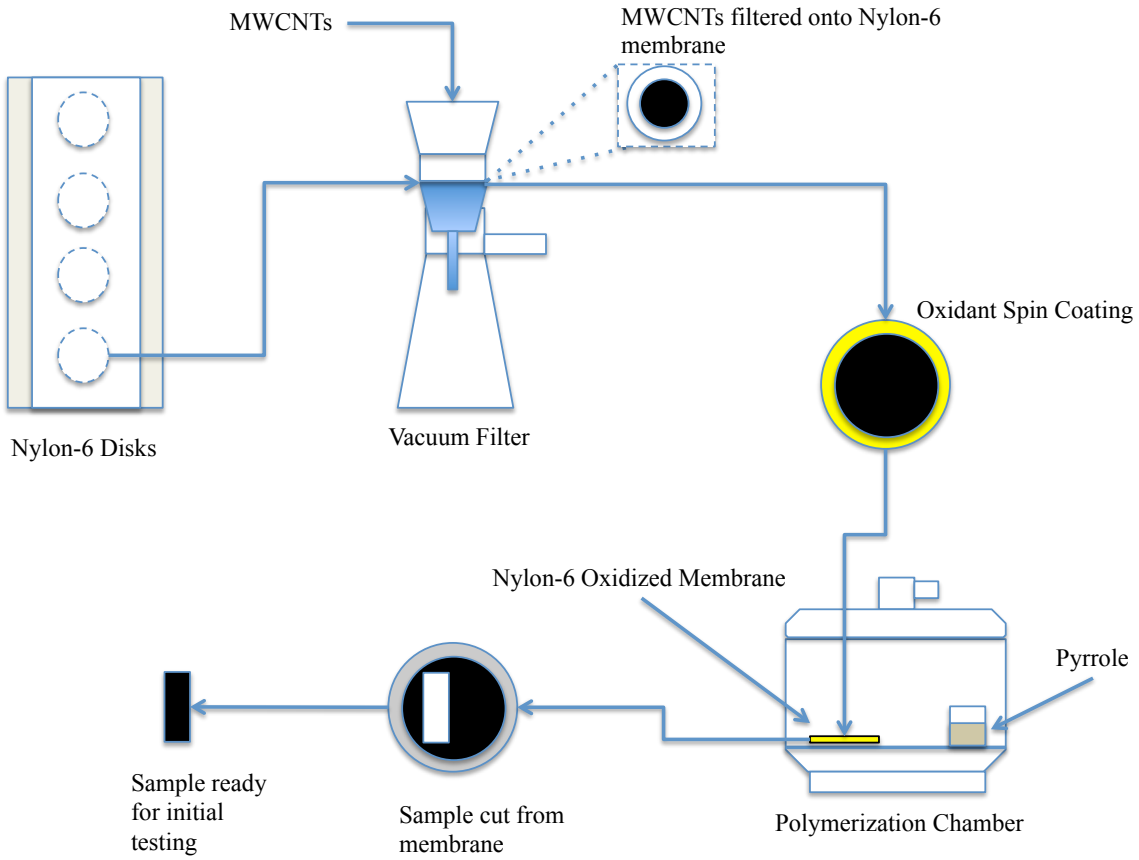

Figure 2. Sensor construction process of Nylon-6 membrane [10].

Once cut from the nylon-6 sheet, the membrane was separated from the paper towel and placed paper towel-side down onto the membrane vacuum funnel. The vacuum funnel was placed in a vacuum flask connected to a vacuum pump with a trap. The trap was cooled by dry ice in isopropanol. Once the membrane was placed on the vacuum funnel, the pump was turned on at full open vacuum and the membrane was wetted with 1-2-milliliters of 0.02-Molar Triton X-114. The top of the funnel was placed onto the membrane and vacuum funnel, then secured with a band of electrical tape and a clamp (seen below, label 1 of Figure 4). The setup was then ready for the addition of the MWCNT solution.

The MWCNT solutions were prepared with 1.9-, 2.1-, or 2.3-milligrams per solution. The MWCNTs were added to a mixture of 34-milliliters of 1.9-millimolar 0.02-Molar Triton X-114 and 216-milliliters of DI water. The mixture was then sonicated with a high-powered sonication horn (label 1 of Figure 3) until the MWCNTs were properly dispersed throughout the solution. The sonicator assembly is shown in Figure 3. Each membrane received 250-milliliters of 1.9-, 2.1-, or 2.3-milligrams of MWCNT solution.

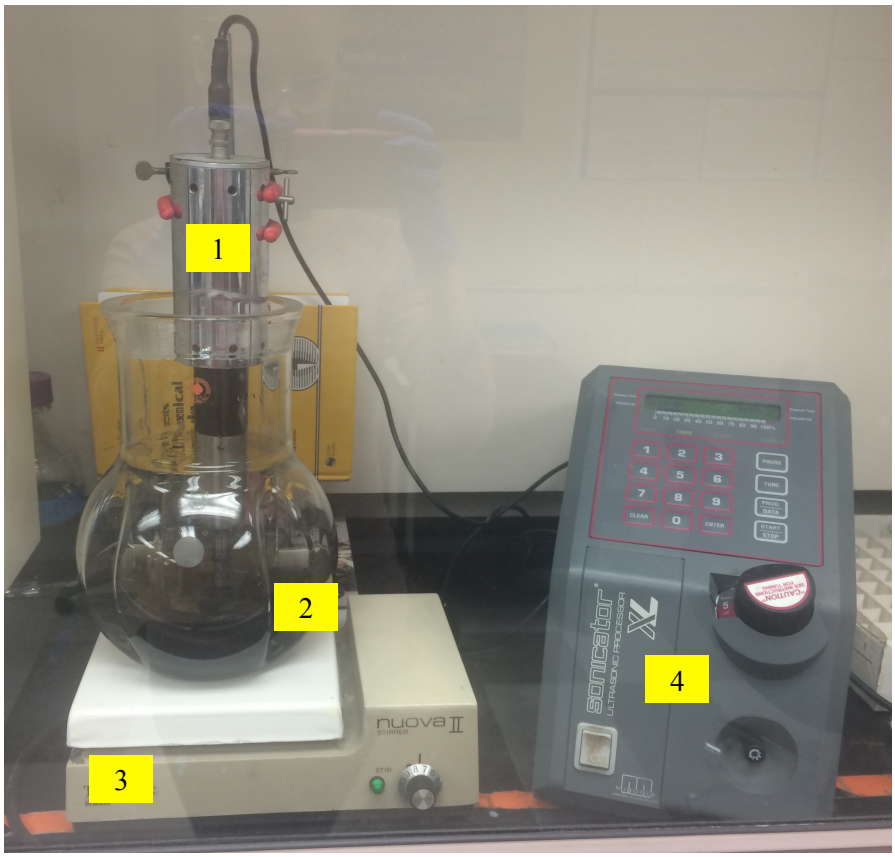

Figure 3. Sonication assembly. 1. High Powered Sonication Horn. 2. MWCNT solution. 3. Stir plate. 4. Misonix Ultrasonic Processor XL.

Once the nanotube solution was added to the funnel (Figure 4, label 1), the vacuum was increased to 5-inches mercury. When the nanotube solution finished filtering, the MWCNTs and membrane were washed with two 25-millitliter aliquots of DI water followed by 25-milliliters of acetone. When the rinse was complete, the membrane was dried with nitrogen for 5-10-minutes, remaining in the funnel during drying to prevent shrinkage. The MWCNT functionalized membrane was removed from the vacuum filtration assembly and allowed to dry in a desiccator for 24-hours. The complete setup can be seen in Figure 4.

After the 24-hour dry-time in the desiccator, the membrane was spin coated with an oxidant. Two oxidants of varying concentration were chosen for this experiment, APS $FeCl_3$ The oxidant was varied from 50-, 75-, and 100-millimolar. A 1-milliliter aliquot of the oxidant was applied using spin coating. The spin coating device was connected to a Philmore regulating transformer power source (model 48-1205) set to 36-volts. The membranes were let to dry in the desiccator for 24-hours. Once dry, the membranes were polymerized with polypyrrole. Polypyrrole was polymerized using the monomer, pyrrole. The membranes were placed in the polymerization chamber with 1-milliliter of pyrrole in a small beaker and the samples surrounding that beaker. Vacuum was applied until 30-inches mercury of vacuum was reached. The samples were left in the polymerization chamber for 48-hours.

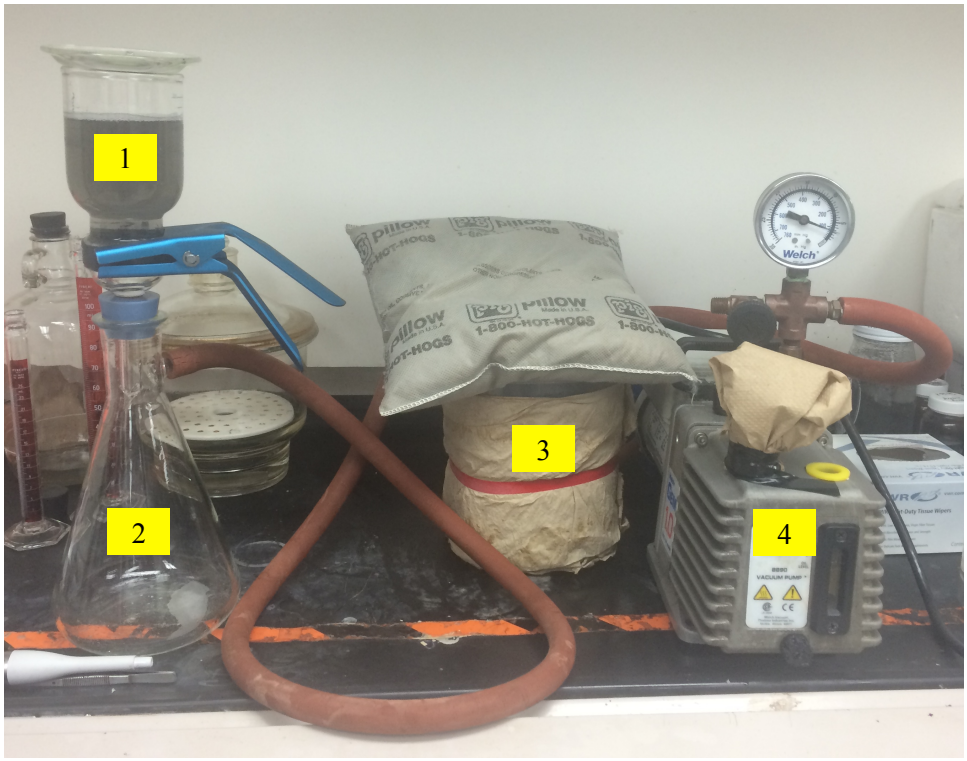

Figure 4. Vacuum filtration of MWCNTs onto Nylon-6 membrane. 1. Top funnel covered by watch glass with 250-mL MWCNT solution. 2. Vacuum flask. 3. Trap submerged in isopropanol and dry ice. 4. Welch Gem B290 vacuum pump.

E. Sensor Testing

Two samples were cut from each polymerized membrane and labeled "A" and "B". The chosen sample was placed in the control box, seen in Figure 5, such that the smooth alligator clips (label6) grasp the sensor sample (label 5) and the serrated alligator clips (label 7) grasp the input/output pins (labels 3 and 8) of the data logger. The temperature probe sits just above the sample; its wire can be seen attached to the control box (label 10). The control box contains a heating element at its base to control the temperature. The dry air inlet can be seen entering the control box at the bottom left (label 2), and the humid air at the top left (label 1). The air outlet exits on the right of the control box (label 9) [11]. **Figure 6** shows the entire testing system, including humidity measurement and data logger (label 1), control box (label 2), JKEM temperature controller (label 3), and humid/dry air flow rates (label 4).

Each sensor sample is first tested at 25°C and 0% RH from -700-millivolts to 700-millivolts using a Solartron 1470E Multichannel Potentiostat/Galvanostat (with Cell Test software) system to plot the sensor's current-voltage curve. The relative humidity was measured using an Omega Engineering data logger (**Figure 6**, label 1). If the sample produced a linear I-V curve, indicating the sensor demonstrated purely electrically-resistive behavior, the sample was then put through a temperature ramp at a constant 700-millivolts. The current was also measured during the ramp. They were ramped from 25°C

until the temperature reached 45°C. The ramp was constructed such that the temperature was increased and held at each 4°C interval for 2-hours. When increasing 4°C between the hold temperature, the rate was 60-degrees per hour. Once 45°C was reached, the temperature ramped back down to 25°C in 4°C intervals at a rate of 60-degrees per hour, resting at each temperature interval for 2-hours. Data for the temperature ramp was recorded by both the JKEM (J-KEM Scientific model Apollo), which recoded the temperature and Solartron 1470E systems, which recorded the resistance change. Resistance and temperature vs. time were recorded for the temperature ramp and the data was combined to illustrate a resistance vs. temperature relationship.

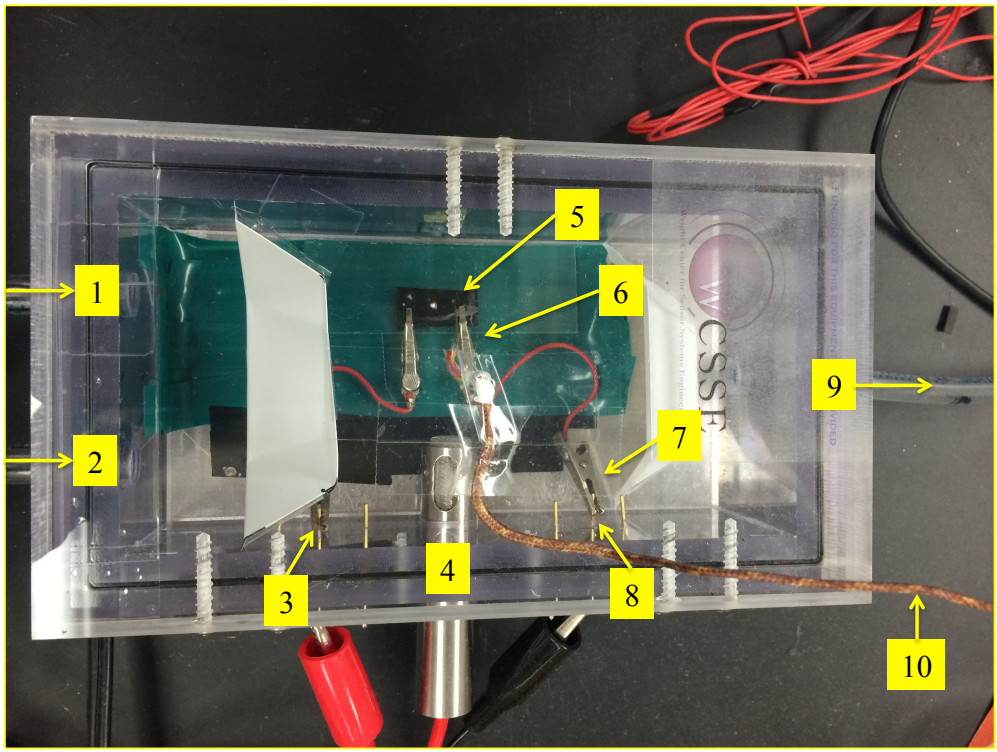

Figure 5. Controller box containing test sample and heating element, used to control temperature and humidity. 1. Humid air inlet. 2. Dry air inlet. 3. Data logger input pin. 4. Humidity probe. 5. Sensor. 6. Smooth alligator clip attached to sample. 7. Serrated alligator clip attached to data logger input/output pins. 8. Data logger output pin. 9. Air outlet. 10. Temperature probe (enters control box just above smooth alligator clips).

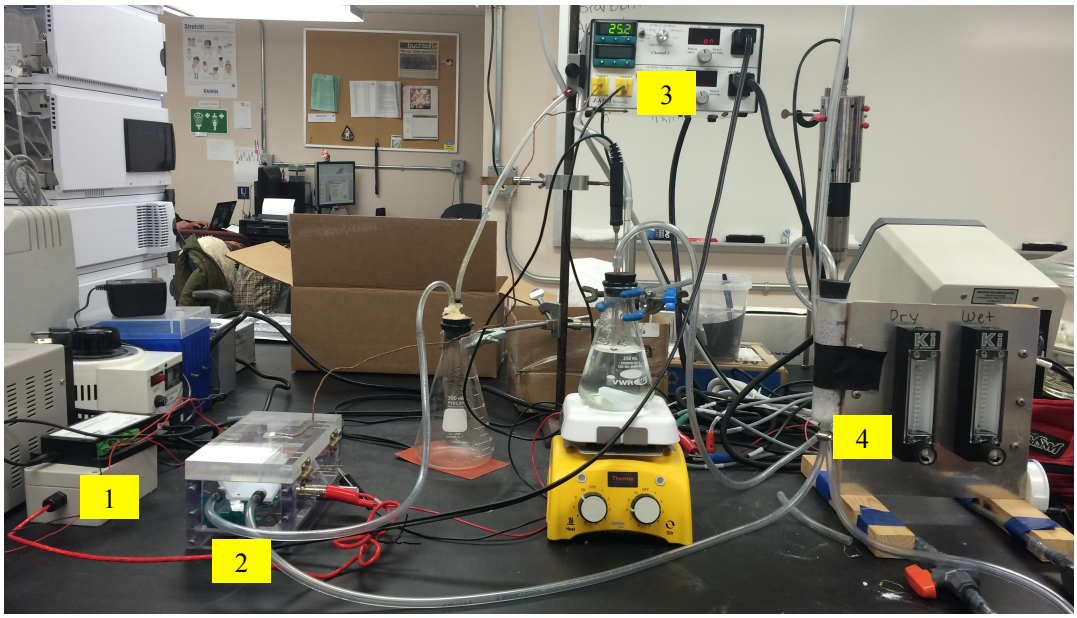

Figure 6. Sensor testing system temperature control and humidity control. 1. Humidity probe (Omega Engineering HX15 (USA)) and data logger (OM-CP- QUADPROCESS-25MA). 2. Controller box containing test sample and heating element, used to control temperature and humidity. 3. Temperature control for JKEM computer data collection. 4. Humidity control – dry/wet air flow measurement and control by Key Instruments, air dried by Drierite anhydrous calcium sulfate [11].

IV. Data and Results

A. Initial Sensor Characterization

The sensors were initially tested for a linear IV curve. The IV curve was run using the Cell Test system at a constant 25°C from -700-millivolts to 700-millivolts. A successful The typical linear IV curve can be seen in Figure 7. The linearity of the IV curve may indicate a complete polymerization of the sensor and a sufficient MWCNT network connection.

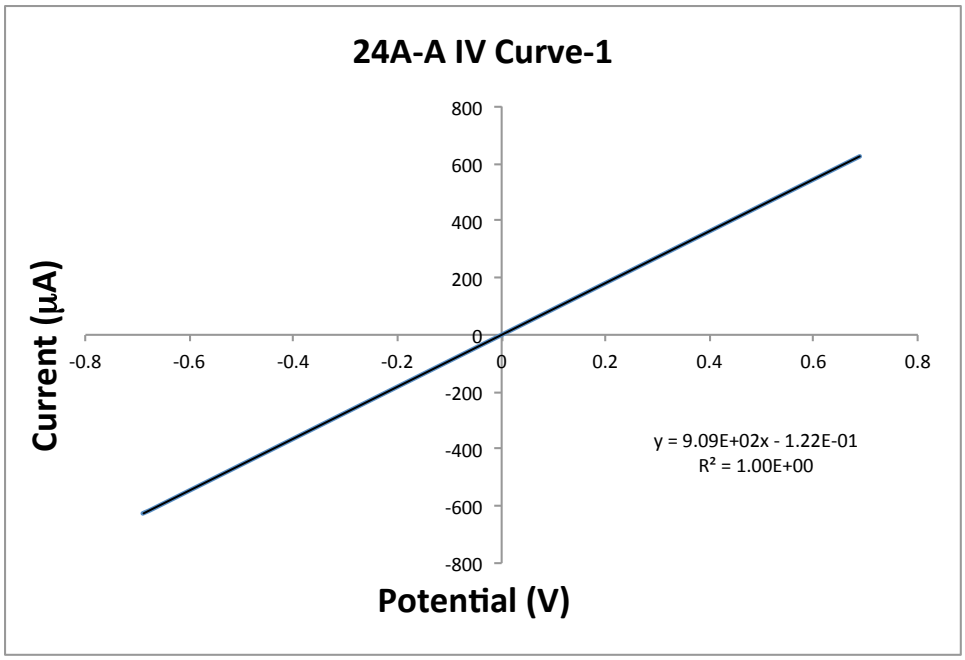

Figure 7. Linear IV curve of sample at constant temperature from -700-mV to 700-mV – sample 24A-A.

Figure 8 shows a non-linear IV curve. This sensor may be acting like a capacitor. Future work will be conducted where the samples will be analyzed using electrochemical impedance spectroscopy to determine if it is acting as a capacitor.

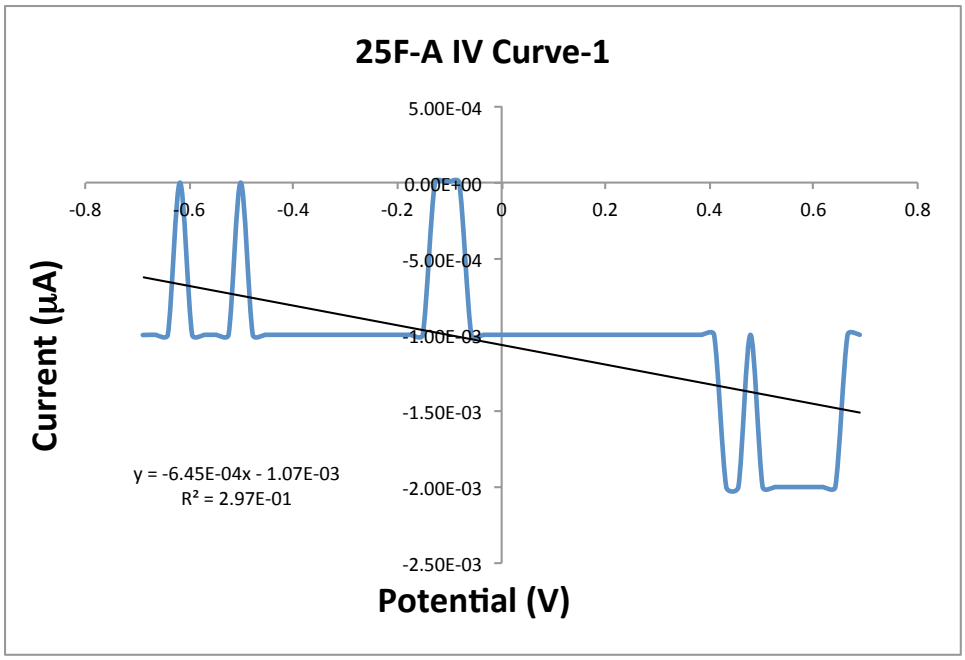

Figure 8. Non-linear IV curve at constant temperature from -700-mV to 700-mV – sample 25F-A.

The initial sensor testing also produces resistance vs. voltage curves. The resistance was calculated using Ohms' Law from the data retrieved from the Cell Test system. An example of this curve is below in Figure 9. Some sensors will drift as the voltage is changed from -700-millivolts to 700-millivolts. The drift is the difference between the

resistance at the beginning of the test and the resistance at the conclusion of the test. The slope of the resistance vs. potential may be used predict whether significant drift will occur during the temperature ramp. As seen in Figure 9, the resistance drift was relatively small, approximately 0.9-ohms, which is only 0.08% of the resistance displayed by the sensor.

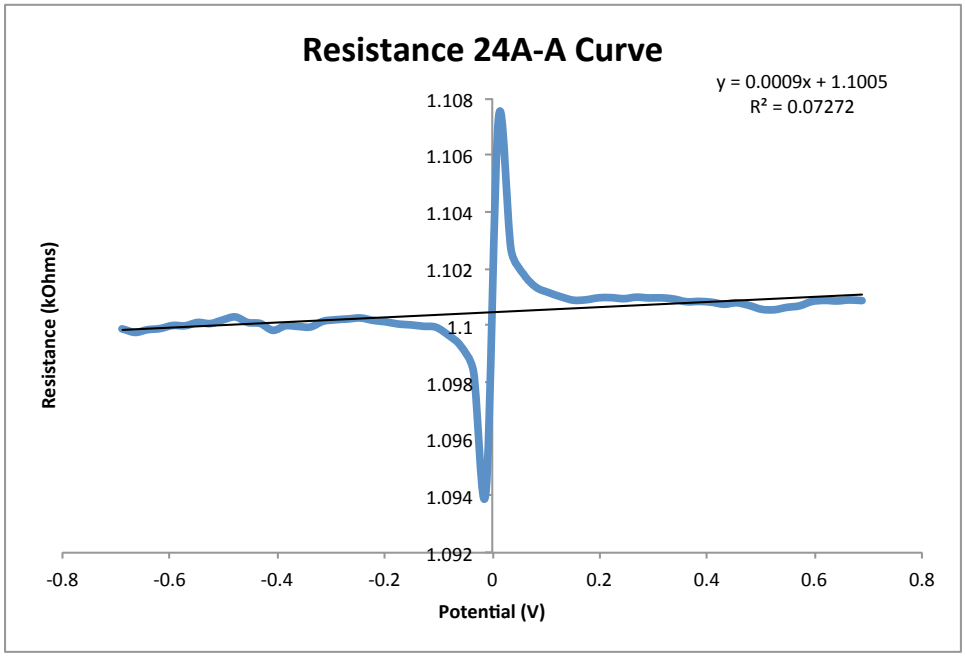

Figure 9. Resistance curve at constant temperature from -700-mV to 700-mV with small slope – sample 24A-A.

The sensor 28B-A also produced favorable results. Figure 10 and Figure 11 are the IV and resistance curves for sensor 28B-A.

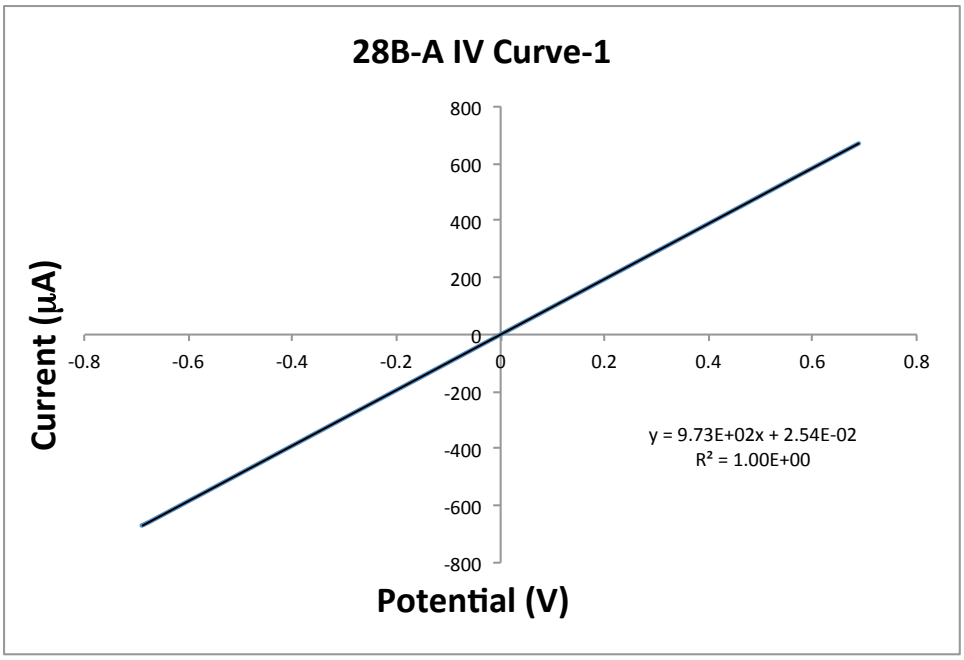

Figure 10. Successful linear IV curve of sample at constant temperature from -700-mV to 700-mV – sample 28B-A.

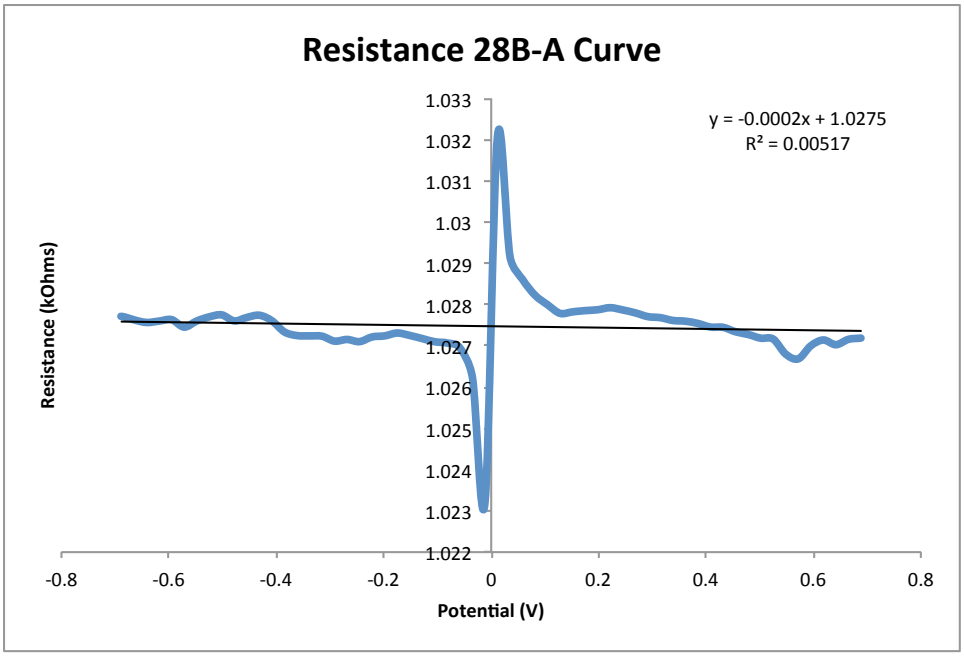

Figure 11. Resistance curve at constant temperature from -700-mV to 700-mV with small slope – sample 28B-A.

Like sensor 24A-A, the IV curve is highly linear and the resistance tread line is nearly horizontal.

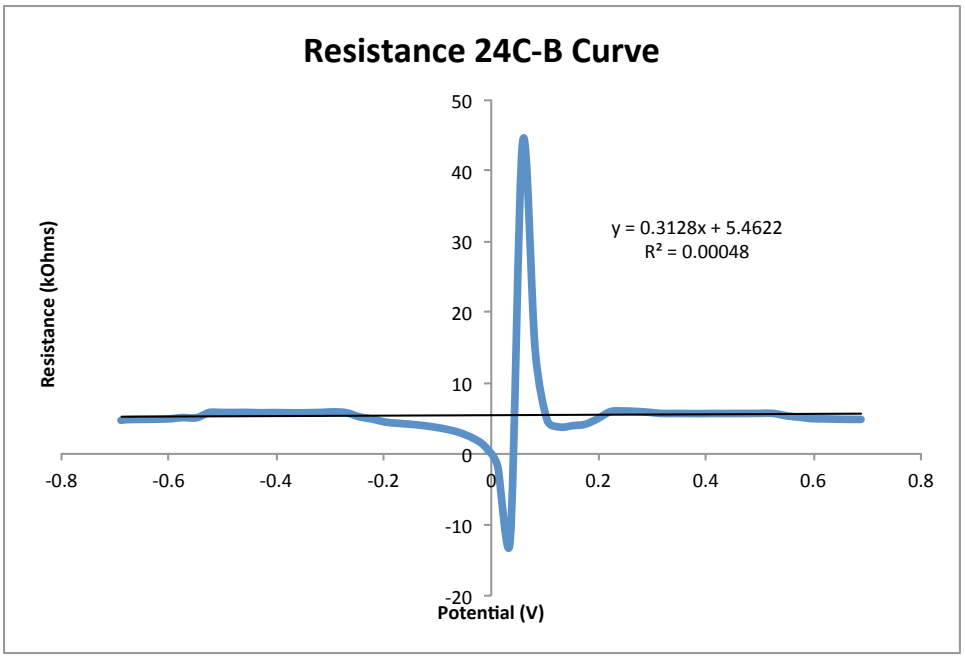

Figure 12. Resistance curve at constant temperature from -700-mV to 700-mV with larger slope – sample 24C-B.

B. Temperature Ramp

If the sensor produced a linear IV curve, it moved to the second phase of testing, a temperature ramp from 25°C to 45°C back to 25°C at constant 700-millivolts. Figure 13 depicts a sensor behaving as desired. There is minimal drift, and clear step resistance changes with the temperature changes. The drift is the difference between the resistance at the beginning and end of the ramp; during the temperature ramp, the sensor will begin and finish at 25°C. The red line corresponds to the temperature ramp, and the blue line corresponds to the resistance response over time.

The temperature/resistance graph was also studied for the temperature ramp. Figure 14, sensor 24A-A, displays a sensor that has a low % hysteresis, approximately 0.0567%.

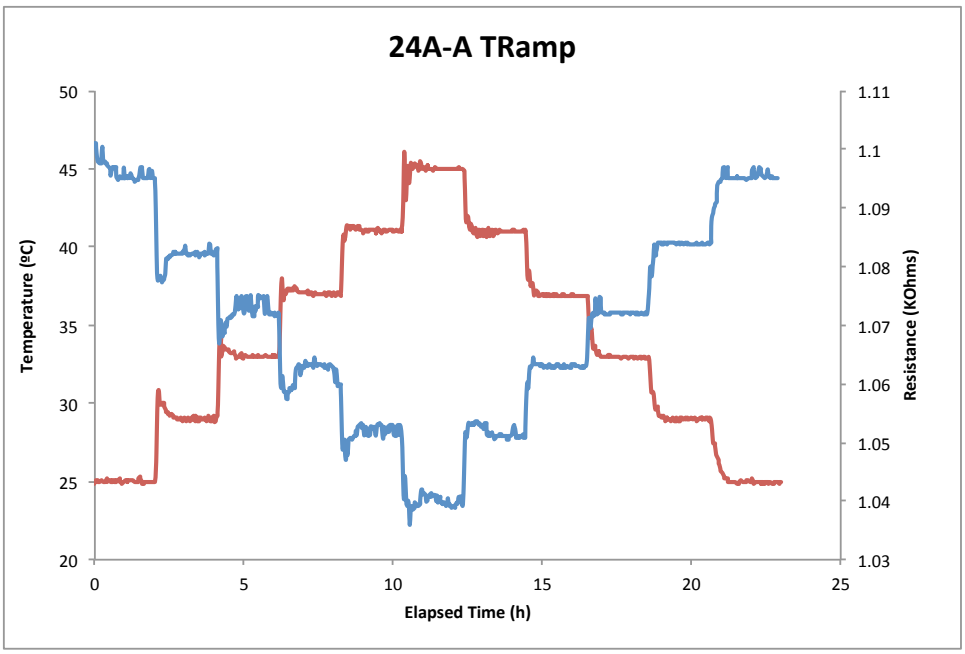

Figure 13. Temperature ramp from 25°C to 45°C to 25°C at constant 700-mV of sample with small drift. Temperature ramp vs. time is red curve and resistance vs. time is blue curve. Sensor 24A-A.

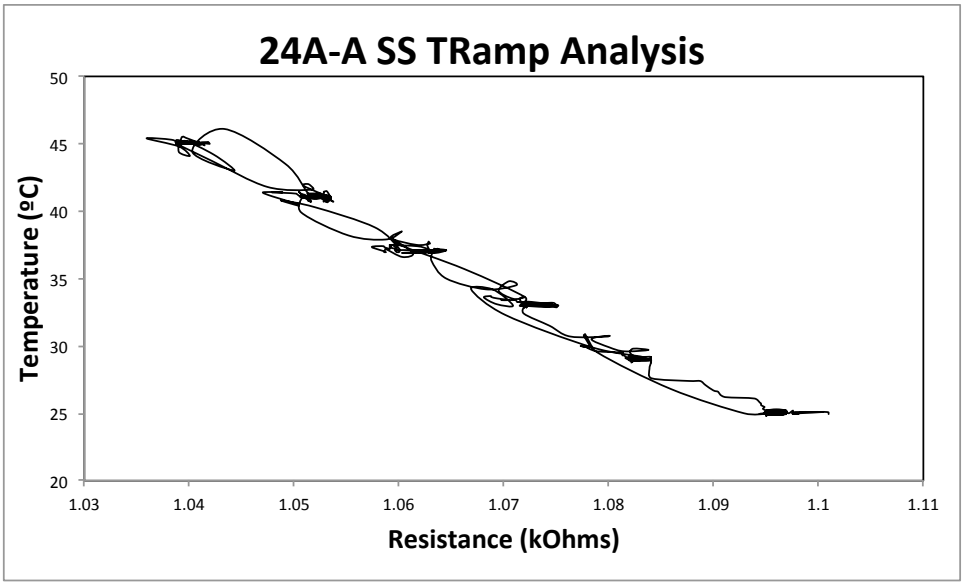

Figure 14. Temperature/resistance graph of temperature ramp of sample with small drift from 25°C to 45°C to 25°C at constant 700-mV. Sensor 24A-A.

Figure 15 displays sensor 28B-A's response to the temperature ramp.

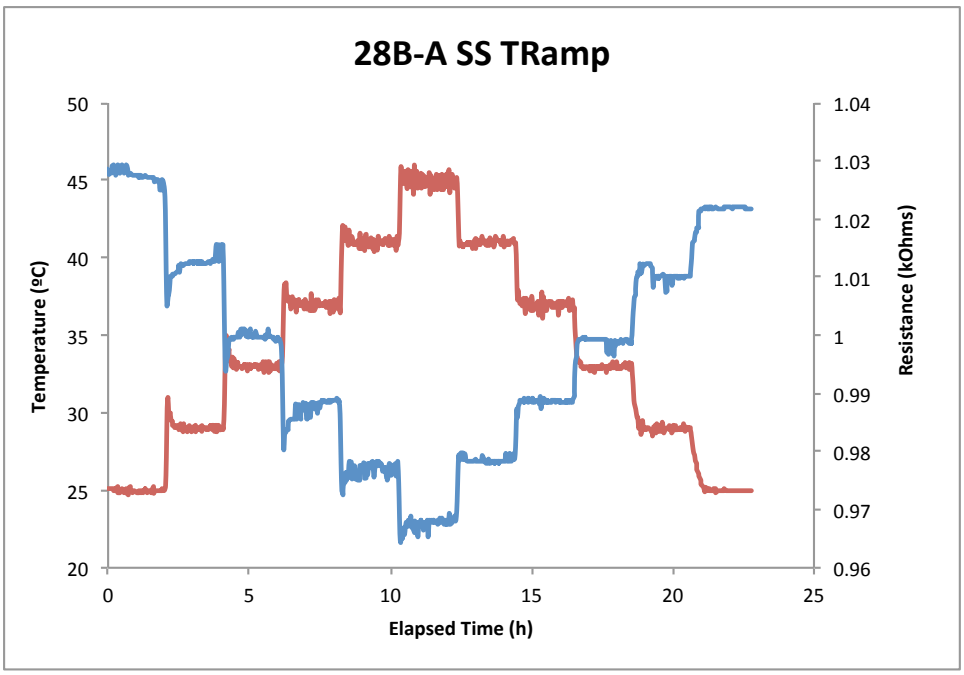

Figure 15. Temperature ramp from 25°C to 45°C to 25°C at constant 700-mV of sample with small drift. Temperature ramp vs. time is red curve and resistance vs. time is blue curve. Sensor 28B-A.

As seen above, there is minimal drift from the beginning of the ramp and the conclusion of the ramp. The responses adjust quickly and efficiently to the temperature change. Figure 16 below is the temperature/resistance graph of sensor 28B-A.

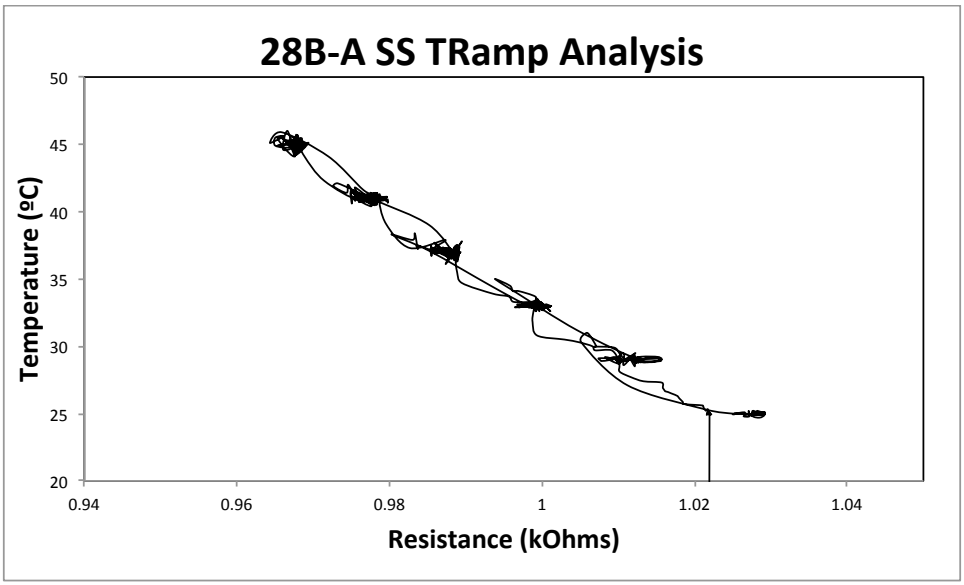

Figure 16. Temperature/resistance graph of temperature ramp of sample with small drift from 25°C to 45°C to 25°C at constant 700-mV. Sensor 28B-A.

The temperature/resistance graph further confirms that there is minimal drift and that resistance remained constant at the hold temperatures both on the up and down ramp.

The temperature ramp for sample 24C-B did not provided as good of results as 24A-A. There was a considerable amount of drift, as seen by the black dashed lines in Figure 17. The steps of the resistance change (depicted in blue) were not as clear and contained a great deal of noise. The % hysteresis is also much higher for sample 24C-B (24.8%). The drift can be seen in the temperature/resistance graph, Figure 18, represented by the red dashed line.

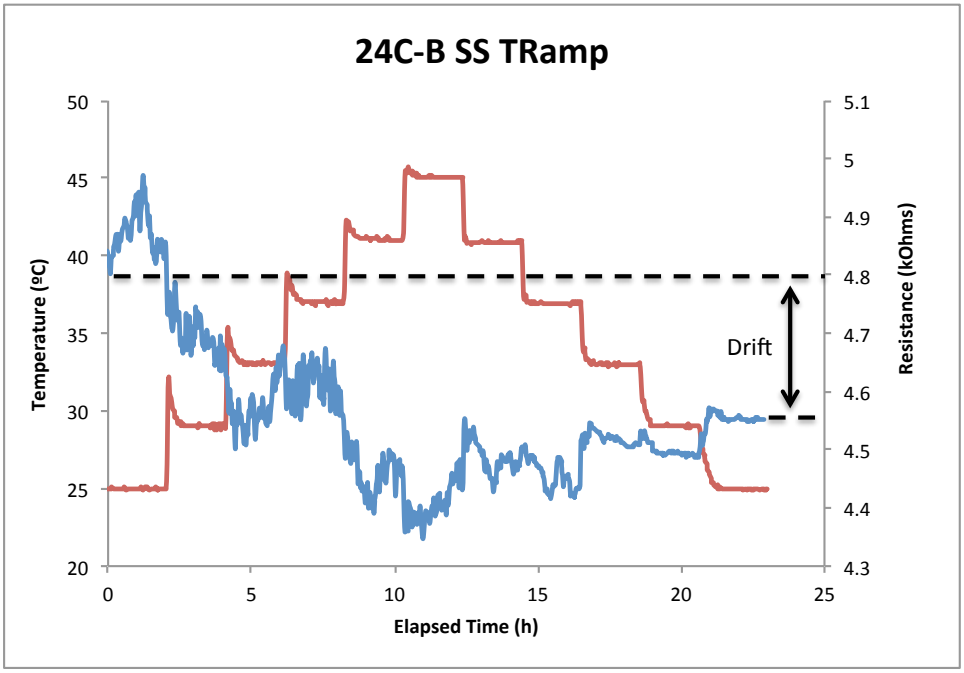

Figure 17. Temperature ramp from 25°C to 45°C to 25°C at constant 700-mV of sample with large drift (marked by dashed line). Temperature ramp vs. time is red curve and resistance vs. time is blue curve.

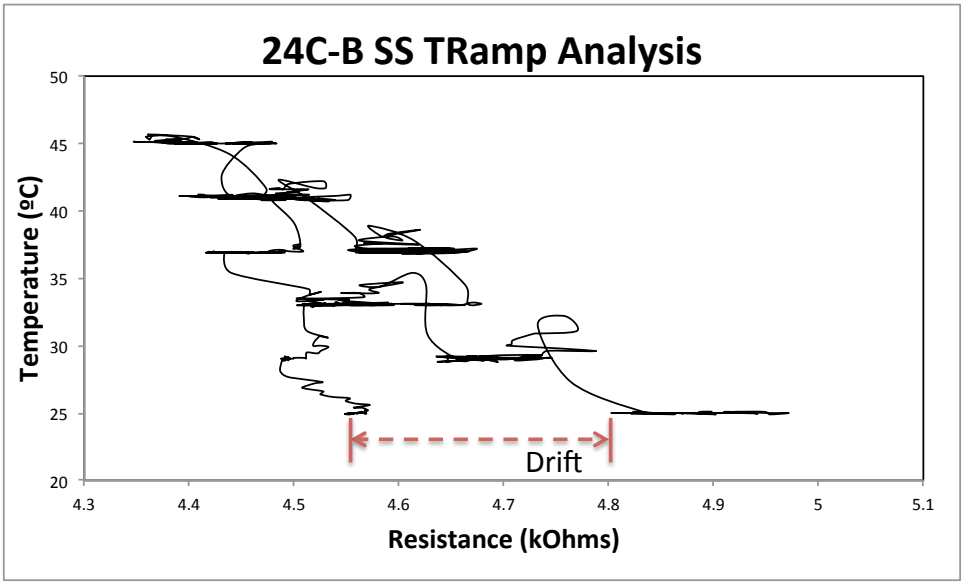

Figure 18. Temperature/resistance graph of temperature ramp of sample with larger drift (marked by red dashed lined) from 25°C to 45°C to 25°C at constant 700-mV.

Some sensors did not respond to temperature change. The cause of this lack of response is unclear, but further analysis will be conducted. Further analysis will include SEM analysis and conductive AFM on non-responsive sensors. Figure 19 shows a sample that is unresponsive to temperature.

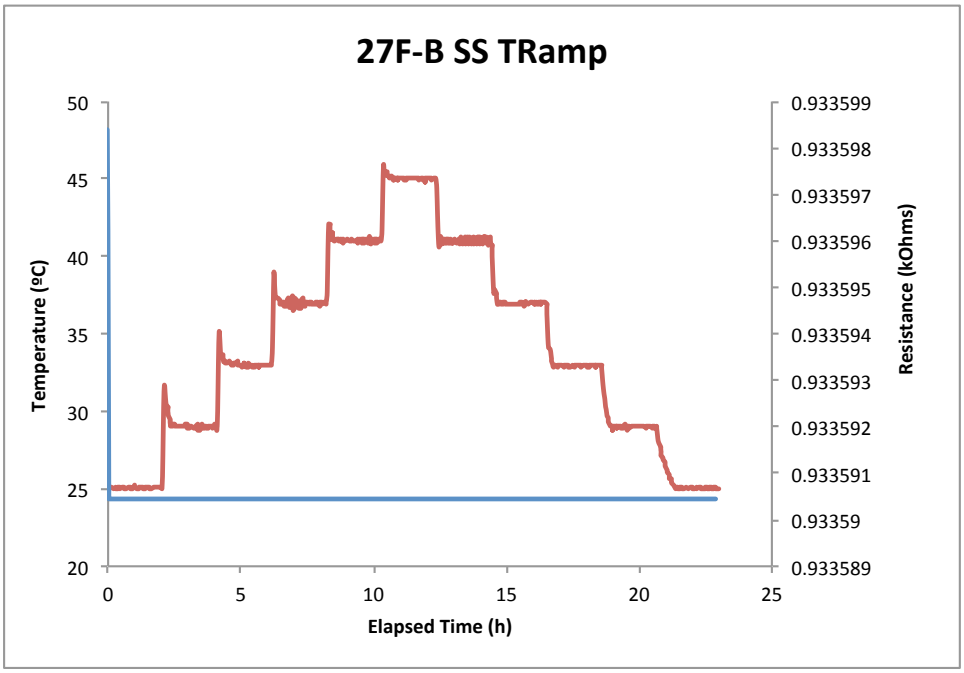

Figure 19. Sensor 27F-B unresponsive to temperature ramp.

V. Discussion and Analysis

A. Initial Sensor Characterization

Sensors that pass the initial testing are characterized by a linear IV curve (an example of such was given as Figure 7). This initial testing is used to verify the linearity of the IV curve, which may indicate a complete polymerization of the sensor and a sufficient MWCNT network connection. The material was appeared to follow Ohms' Law, so linear IV curve was observed.

Equation 3

$$V = IR$$

which produces a linear current (I) – voltage (V) curve where the slope is resistance (R). As seen by Figure 7, the assumption that the material adheres to Ohms' Law was valid.

However, some materials were found to deviate from Ohms' Law. This behavior was seen in Figure 8. This deviation may be due to clumping of the nanotubes or if the nanotubes were not distributed properly during filtration. The deviation may also be due to incomplete/ non-uniform polymerization. It is hypothesized that when a sensor sample

is incompletely polymerized, the network of MWCNTs is disconnected and may act as a capacitor. The peaks of the graph in Figure 8 may be depicting a building charge and the rapid release of this charge. A pictorial explanation of the effect of incomplete polymerization on the IV curve can be seen in Figure 20. The electrons flow from the negative terminal to the positive terminal; however, they congregate on the border between the polymerized and the non-polymerized regions of the sensor. This congregation could be caused by the disconnected network of MWCNTs past this border in the non-polymerized section of sensor. Eventually, the charge is built up enough that it must be released, causing the peaks seen in Figure 8.

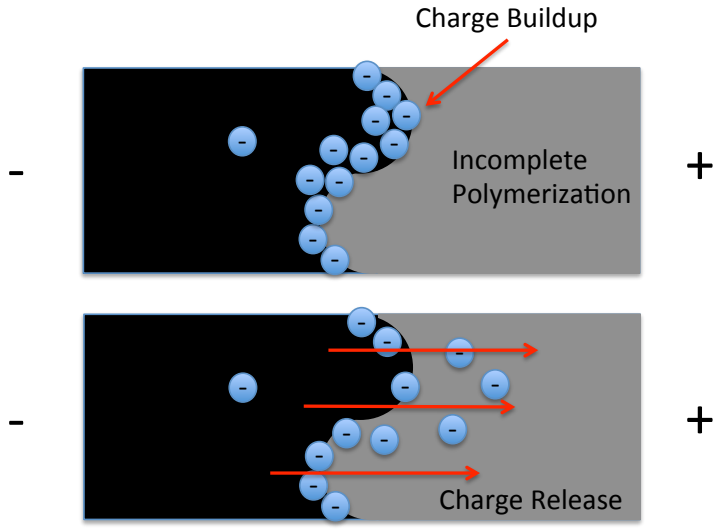

Figure 20. Capacitor behavior of sensor with incomplete polymerization. The electrons migrate towards positive terminal and build up on the polymerized/non-polymerized border (top figure). Enough charge build-up results in the discharge of electrons (bottom figure).

The incomplete polymerization of the sensors may have been caused by a number of reasons. One of which can be traced back to the oxidation stage of sample preparation. Since the oxidant's main purpose is to cause the polymerization of pyrrole to polypyrrole, if the oxidant was not properly dispersed during spin coating, the result may have been incomplete polymerization. The sample could also have been unevenly coated when in the polymerization chamber due to loss of vacuum.

The resistance vs. voltage slope may be used to determine future behaviors of the sensor, as discussed in the following section.

B. Temperature Ramp

Generally, the sensors that have a greater change in resistance in their resistance/voltage curves will drift considerably in the temperature ramp as well. This trend was seen with sample 24C-B, shown in Figure 12 and Figure 17, the drift marked by black dashed lines in Figure 17. The sensor drifted during the potential ramp and continued to drift during the temperature ramp. Conversely, the resistance change in sensor 24A-A's resistance/voltage curve is very small, which correctly predicts that the drift during the temperature ramp would also be very small (Figure 9 and Figure 13). If

the sensors continue to drift every time they are heated, i.e. when placed in a shoe or prosthetic socket during exercise, their applicability would be limited. However, there is the possibility that some of the sensors require an annealing process, and after the initial ramp the sensor would be stable and greatly reduce the drift., Reduction of drift may also occur by changing the polymer or oxidant used for the process.

There is also a considerable amount of "noise" in sensor 24C-B's resistance response to temperature. The steps are not clearly defined as they are for 24A-A. This may be caused by a network disconnect of the MWCNTs within the sensor. The charge builds up along the edges of the disconnect and releases. Figure 8 is an extreme example of this. However, many of the graphs tend to develop more defined steps with less noise as they near the end of the temperature ramp. This is evidence supporting the hypothesis that an annealing step could be needed to stabilize the sensor response.

The drift is also evident in the Temperature/resistance graphs of Figure 14 and Figure 18. The Temperature/resistance is the similarity between the up ramp and down ramp resistances. Sensor 24A-A has a very small % hysteresis, 0.0567%, so the up ramp is nearly indistinguishable from the down ramp. Sensor 24C-B, however, has a much larger % hysteresis, 24.8%. The graph shown in Figure 18 has clearly defined up and down ramps. The red dashed line marks the drift in this graph.

As seen by Figure 13 and Figure 17, the resistance is inversely related to temperature; as temperature increases, the resistance decreases. This characteristic is known as the Negative Temperature Coefficient (NTC). Metals typically display Positive Temperature Coefficients (PTC).

C. Parameter Dependence Graphs

Plots of each of the variables (polymer weight percent, MWCNT loading, and oxidant type and concentration) versus the selected parameters (alpha-values, resistance change, and % hysteresis) are presented below. The average values of each of the variables were plotted against the average of each parameter. Error bars were included to show the deviation of points from the mean (plotted) value.

There was a notable difference between the measured value of the MWCNT loading and the target values. The measured weight was determined by weighing the PA6 membrane before and after the MWCNTs were vacuum filtered onto the membrane. Table 2 compares the measured and desired MWCNT loading. The below values are in the order of their filtration, and the bold lines indicate the preparation of new batch.

Table 2. MWCNT loading - target vs. measured values.

Sample	MWCNT Loading - Target (mg)	MWCNT Loading - Actual (mg)	Difference (mg)
25F	1.9	2.2	0.3
23F	1.9	2.5	0.6

25C	1.9	3.1	1.2
23C	1.9	1.6	-0.3
26A	1.9	2.9	1.0
26B	1.9	2.3	0.4
23D	2.1	2.8	0.7
24A	2.1	3.3	1.2
24B	2.1	3.1	1.0
24C	2.1	2.8	0.7
26E	2.1	4.4	2.3
27D	2.1	3.3	1.2
28A	2.3	2.4	0.1
28B	2.3	2.4	0.1
28D	2.3	2.6	0.3
28E	2.3	2.7	0.4
27E	2.3	2.8	0.5
27F	2.3	2.8	0.5

The deviation from the target value could be caused by a number of reasons. The difference was not necessarily caused by MWCNTs settling at the bottom of the beaker because the difference did not increase in later filtered samples. If this were the case, we would consistently see a greater difference in the later samples, but this is not the case. Human error is definitely a factor to consider, especially when measuring such minute masses.

Another hypothesis is that the Triton X-114 surfactant was depositing on the membrane during vacuum filtration. This theory is supported by Bai et. al., who studied surfactant (namely Triton X-series surfactants) deposition on CNTs [12].

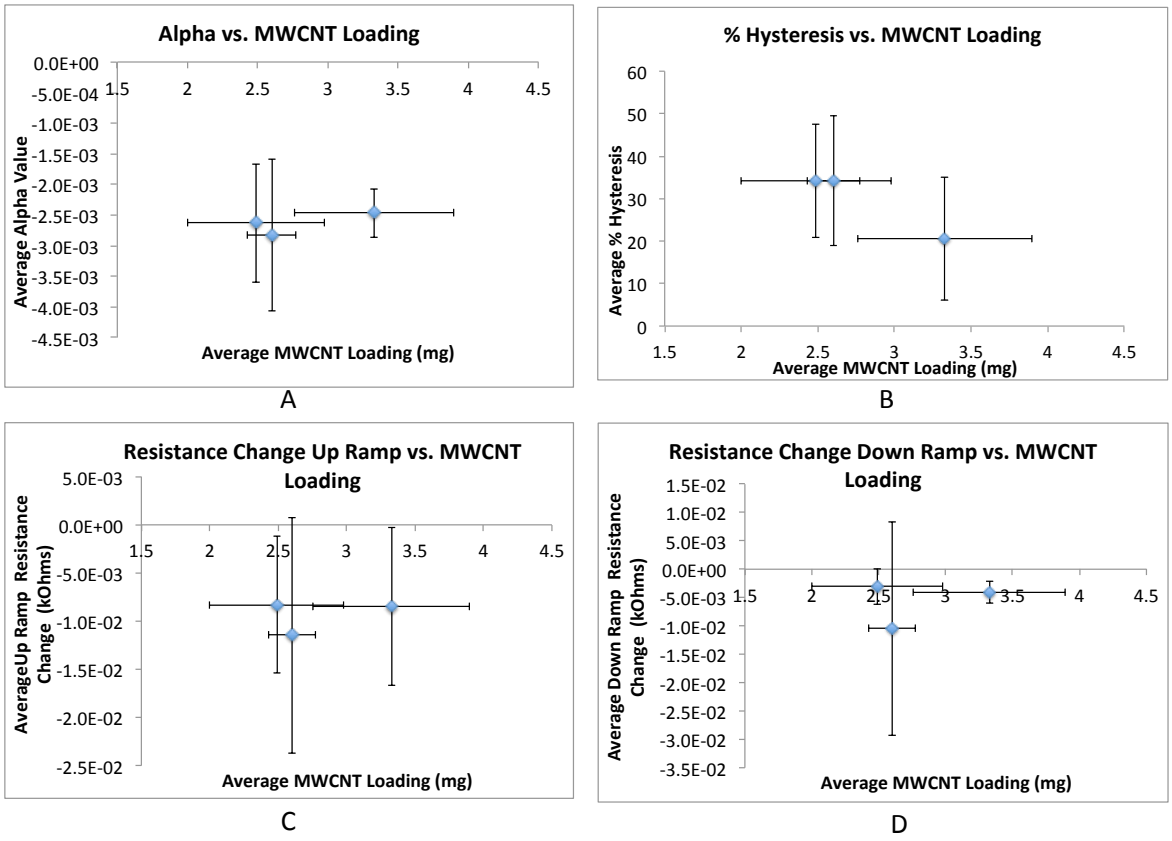

Figure 21.A. Average alpha value vs. average MWCNT loading. B. Average % hysteresis vs. average MWCNT loading. C. Average up ramp resistance change vs. average MWCNT loading. D. Average up ramp resistance change vs. average MWCNT loading.

A large amount of deviation was observed in the comparison of MWCNT loading versus the parameters α-value, % hysteresis, and resistance change. Percent hysteresis showed a loose negative correlation to MWCNT loading.

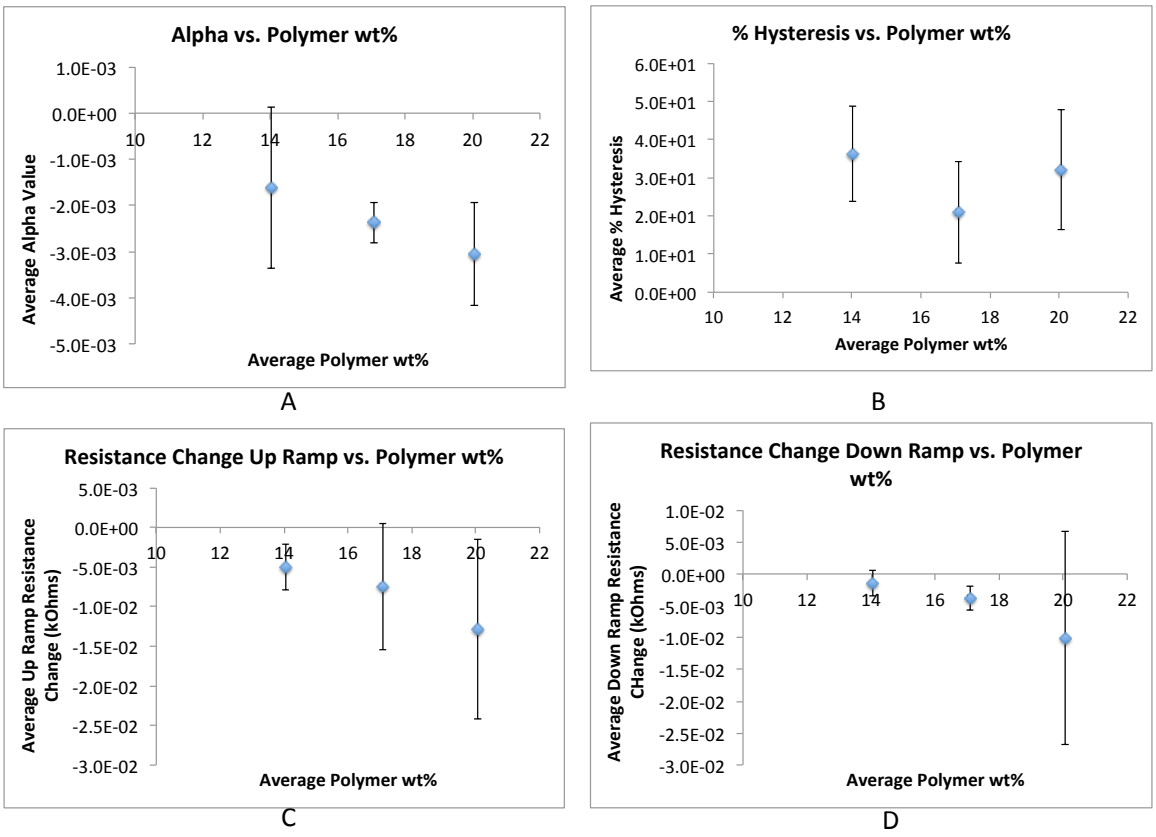

Figure 22. A. Average alpha value vs. average polymer wt%. B. Average alpha value vs. average polymer wt%. C. Average up ramp resistance change vs. polymer wt%. D. Average down ramp resistance change vs. average polymer wt%.

The measured values of the polymer wt% of the electrospun material was very close to the target value, and there was little deviation in actual wt% between the two materials created for each target wt%. The α-value seems to become more negative as polymer wt% increases, as well as the change in resistance of the up and down ramp.

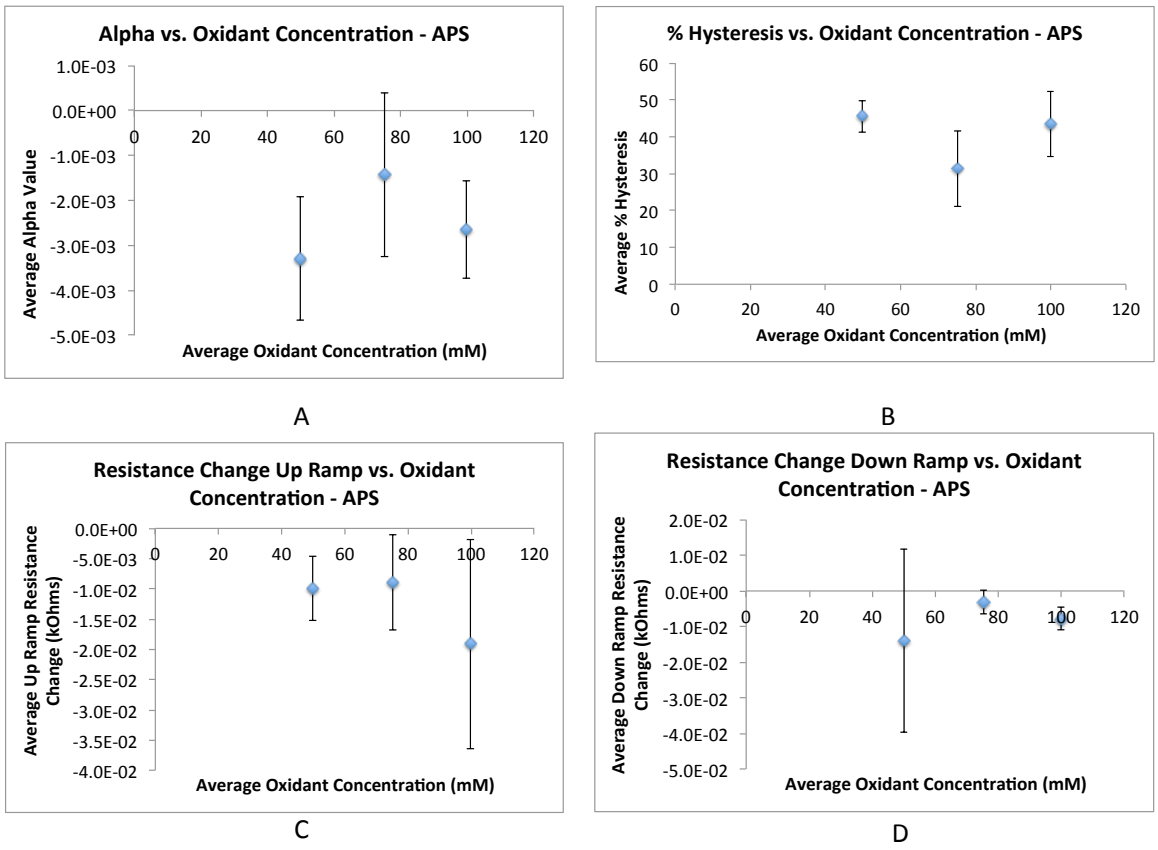

Figure 23. A. Average alpha value vs. average APS concentration. B. Average % hysteresis vs. average APS concentration. C. Average up ramp resistance change vs. average APS concentration. D. Average up ramp resistance change vs. average APS concentration.

The oxidant concentrations for APS were close to the target concentrations with little variation. None of the correlations presented appear to be linear, however, other correlations may emerge after further analysis and testing.

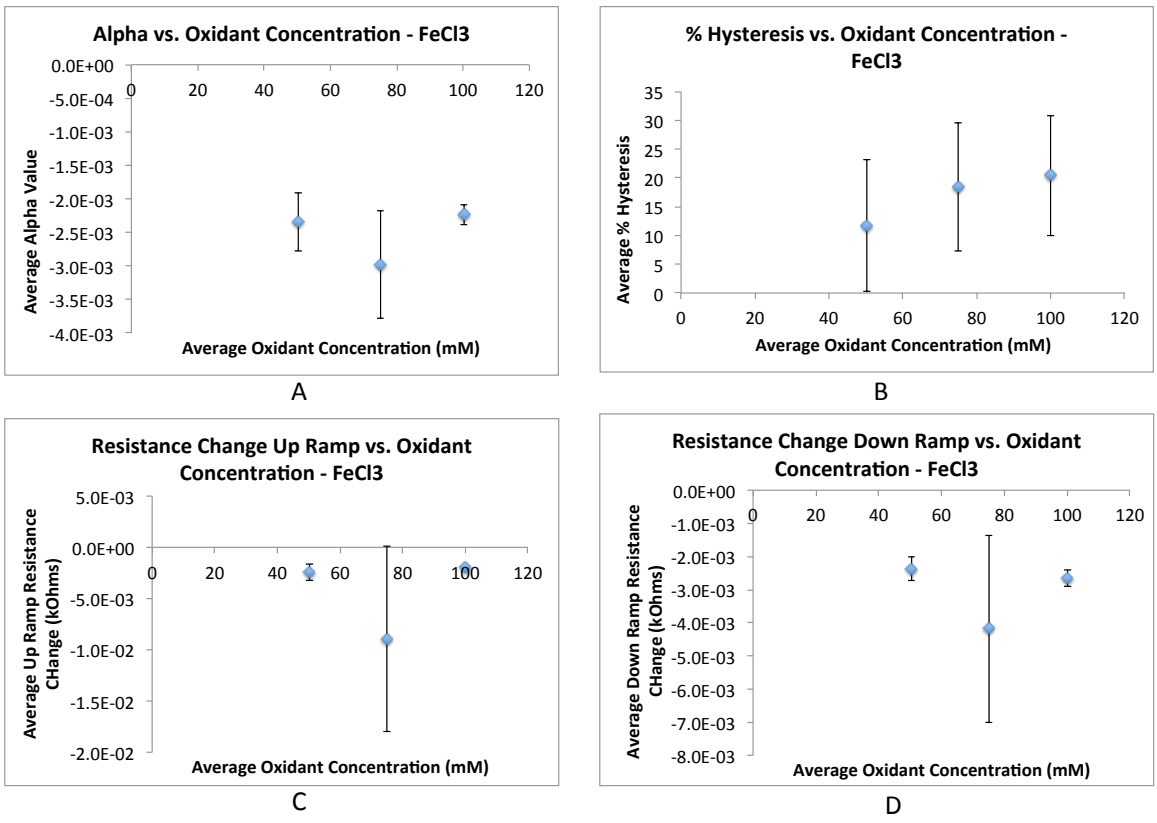

Figure 24. A. Average alpha value vs. average FeCl3 concentration. B. Average alpha value vs. average FeCl3 concentration. C. Average alpha value vs. average FeCl3 concentration. D. Average alpha value vs. average FeCl3 concentration.

Like APS, the oxidant concentrations for $FeCl_3$ were also close to the target concentrations with little variation. The % hysteresis graph shows a possibility for a positive correlation to $FeCl_3$ oxidant concentration.

D. Temperature/Resistance Relation Model

The following equation was used to model the relationship between sensor resistance and temperature:

Equation 4

$$T = -\frac{1}{\alpha}\left(\frac{R}{R_0} - 1\right) + T_0$$

where α is the Temperature Coefficient of Resistance, and R_0 and T_0 are the baseline resistance and temperature. The sensors were compared to the above alpha-based model, which was analyzed for effectiveness to predict the behavior of the sensors.

Sensor 24A-A displayed favorable characteristics such as low amounts of drift and noise, linear IV curve, and quick response and stabilization when temperature changes. In

the equation above, resistance, R, is the independent variable and temperature, T, is the dependent variable; all other terms are constants unique to the sensor. For instance, sensor 24A-A has an α-value of 0.0025, a T_0 (reference temperature) of 25°C, and a reference resistance, R_0, at 25°C of 1.10-kOhms. Figure 25 shows the results of the model compared to the actual data.

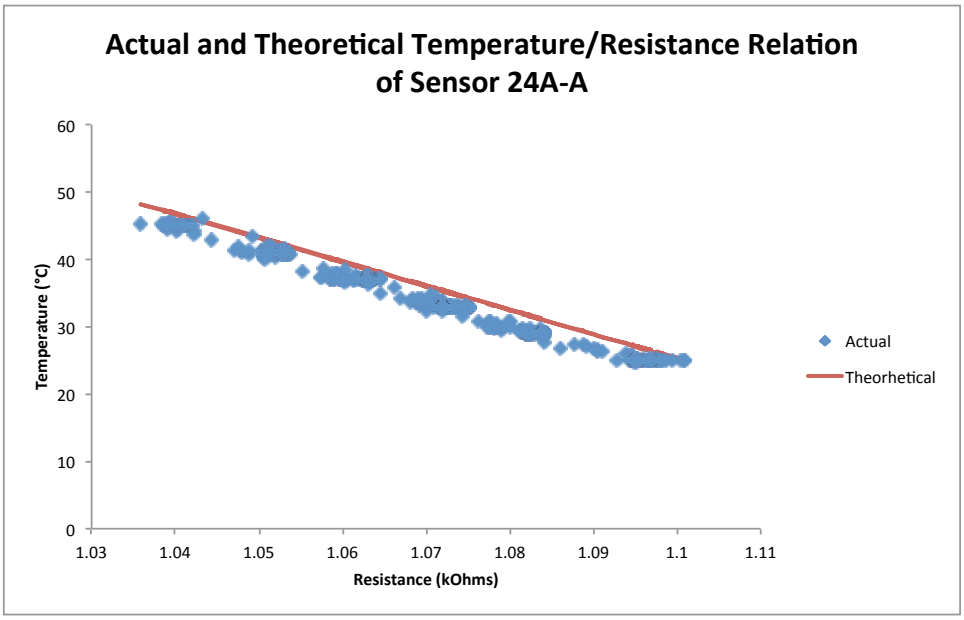

Figure 25. Actual (blue points) and Theoretical (red treadline) temperature relation to resistance of sensor 24A-A.

Figure 26 depicts the relationship between average resistance, both actual and theoretical, and temperature. The temperature was ramped 4°C from 25°C to 45°C and back down to 25°C with a 2-hour hold time at each temperature. Averages that created the below graph were calculated over the hold times at each temperature change. As seen in the chart, the variation of the actual resistance and temperature (represented by the error bars) is very small, indicating a quick and stable response to temperature change.

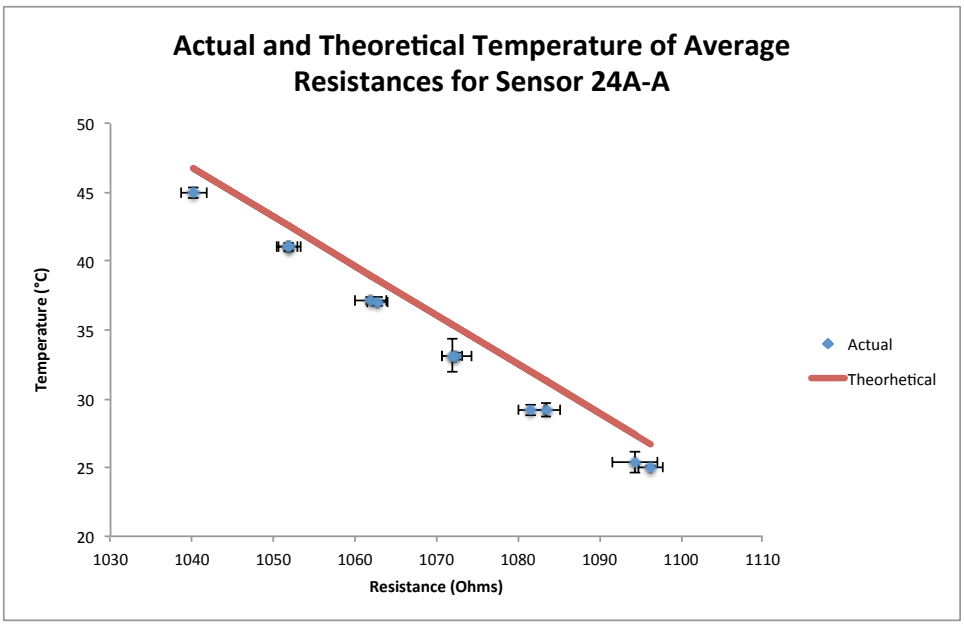

Figure 26. Actual and theoretical temperatures corresponding to average resistances for Sensor 24A-A.

As seen in Figure 25 and Figure 26, the values given by the theoretical model were slightly higher than those measured during testing. Table 3 lists the average temperature difference between the tested data and the model at each hold temperature and the average difference of the entire data set.

Table 3. Temperature difference between values produced by the model and the measured values.

Actual Average Hold Temperature (°C)	Theoretical Average Temperature (°C)	Average Difference (°C)	Percent Relative Error (%)
25.04	26.71	1.67	6.66
29.22	31.93	2.71	9.26
33.12	35.20	2.08	6.27
37.10	38.96	1.86	5.02
41.08	42.60	1.52	3.70
44.99	46.79	1.80	3.99
41.05	42.58	1.53	3.74
36.97	38.56	1.59	4.30
32.99	35.29	2.30	6.98
29.03	31.08	2.05	7.07
25.01	26.99	1.98	7.92
Total: 34.10	36.03	1.93	5.66

The above table shows that the highest average difference in temperature (for sensor 24A-A) occurred during the up 29°C ramp with a difference of 2.71°C and a percent error of 9.26%. The average temperature difference of the data set as a whole was under 2°C with an error of 5.66%.

The correlations seen in Figure 25 and Figure 26 show that the relationship between temperature and resistance is highly linear. The relation of actual to theoretical temperature can be seen in Figure 27.

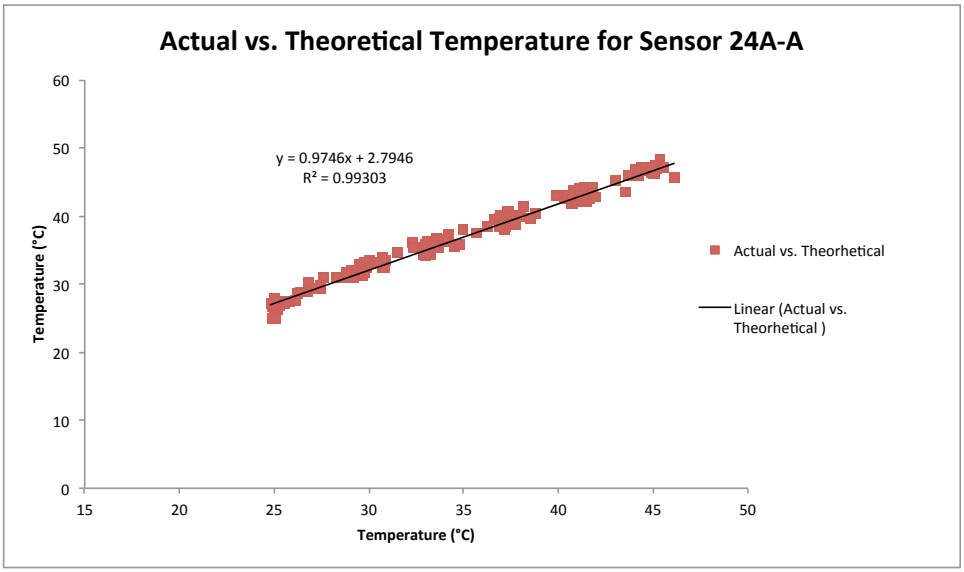

Figure 27. Actual temperature and theoretical temperature relation for Sensor 24A-A.

VI. Conclusions

Sensors 24A-A and 28B-A produced the best responses to temperature change. They both displayed linear IV curves and minimal drift. As seen by their temperature ramp graphs, they respond quickly to temperature change with minimal noise and stabilize quickly. The model presented in this paper returned slightly higher values than the measured values; however, the results were very similar. When compared to sensor 24A-A's data, the model's highest relative error was 9.26% from the actual data, which was an approximately 2.71°C difference at hold temperature 29°C on the up ramp. The average temperature difference of the entire data set was 5.66%, approximately 1.93°C difference.

The results from the parameter dependence graphs showed a possible negative correlation between % hysteresis and MWCNT loading. A negative relation between α-value and polymer wt% was also oserved. The resistance change of both up and down ramps appears to have a loose negative relation to polymer wt%. The % hysteresis graph also shows a possible positive correlation to $FeCl_3$ oxidant concentration. More analysis needs to be conducted on these aspects in order to conclude whether a correlation actually exists between these parameters.

The second part of the DOE will be conducted during the summer of 2015. This portion will explore the effects of MWCNT loading, polymer wt%, and oxidant type and concentration on polyurethane rather than nylon-6. Sensors whose resistance did not respond to temperature will be further analyzed using SEM and conductive AFM. Also further investigation is required to determine whether if surfactant deposits on the MWCNTs and if so, what amount of surfactant deposits and the effects of this deposition on sensor response, sensitivity and resistivity.

VI. Literature Cited

[1] *Glossary Definition for RTD*. Maxim Integrated , n.d. Web. 25 Mar. 2015. <http://www.maximintegrated.com>.

[2] L. B. Hunt, "The Origin of the Platinum Resistance Thermometer," Platinum Metals Rev., vol. 24, no. 3, pp. 104–112, Jul. 1980.

[3] Sen, S.K., T.K. Pan, and P. Ghosal. 2011. "An improved lead wire compensation Technique for conventional four wire resistance temperature detectors (RTDs)." Measurement (02632241) 44, no. 5: 842-846. Academic Search Complete, EBSCOhost (accessed March 25, 2015).

[4] Wujcik, E. K.; Blasdel, N. J.; Trowbridge, D.; Monty, C. N. Ion Sensor for the Quantification of Sodium in Sweat Samples. *IEEE Sensors Journal* **2013**, *13* (9), 3430–3436.

[5] *Nylon 6 (PA) — Polyamide 6*. RTP Company Specialty Compounds , n.d. Web. 25 Mar. 2015. <http://www.rtpcompany.com>.

[6] M. De Volder, D. Reynaerts, C. Van Hoof, S. Tawfick, and A. J. Hart, "A temperature sensor from a self-assembled carbon nanotube microbridge," in Sensors, 2010 IEEE, 2010, pp. 2369–2372.

[7] Sliman, Almuhamed, Nabyl Khenoussi, Laurence Schacher, Henri Balard, and Dominique C. Adolphe. "Measuring of electrical properties of nano-web of PAN containing MWNT." *The Fiber Society 2010 Fall Meeting and Technical Conference* (October 20, 2010). Accessed March 25, 2015. http://www.academia.edu.

[8] Yang, Lingfang, Zhou Shi, and Wenhao Yang. "Polypyrrole directly bonded to air-plasma activated carbon nanotube as electrode materials for high-performance supercapacitor." *Electrochimica Acta* 153 (2015): 76-82. Elsevier.

[9] Peng, Yu-Jung, Tzu-Ho Wu, Chun-Tsung Hsu, Shin-Ming Li, and Ming-Guan Chen. "Electrochemical characteristics of the reduced graphene oxide/carbon nanotube/polypyrrole composites for aqueous asymmetric supercapacitors." *Journal of Power Sources* 272 (2014): 970-78. Elsevier.

[10] Blasdel, Nathaniel. "SSCS Sensor Construction Procedure."

[11] Blasdel, Nathaniel J., Evan K. Wujcik, Joan Carletta, Kye-Shin Lee, and Chelsea N. Monty. "Fabric Nanocomposite Resistance Temperature Detector." *IEEE Sensors Journal*.

[12] Bai, Yingchen, Daohui Lin, Fengchang Wu, Zhenyu Wang, and Baoshan Xing. "Adsorption of Triton X-series surfactants and its role in stabilizing multi-walled carbon nanotube suspensions." *Chemosphere* 79 (2010): 362-67.